

TIC: A Stokes inversion code for scattering polarization with partial frequency redistribution and arbitrary magnetic fields

H. LI,^{1,2} T. DEL PINO ALEMÁN,^{1,2} J. TRUJILLO BUENO,^{1,2,3,*} AND R. CASINI⁴

¹*Instituto de Astrofísica de Canarias, E-38205 La Laguna, Tenerife, Spain*

²*Departamento de Astrofísica, Universidad de La Laguna, E-38206 La Laguna, Tenerife, Spain*

³*Consejo Superior de Investigaciones Científicas, Spain*

⁴*High Altitude Observatory, National Center for Atmospheric Research.
P.O. Box 3000, Boulder, CO 80307-3000, U.S.A.*

ABSTRACT

We present the Tenerife Inversion Code (TIC), which has been developed to infer the magnetic and plasma properties of the solar chromosphere and transition region via full-Stokes inversion of polarized spectral lines. The code is based on the HanleRT forward engine, which takes into account many of the physical mechanisms that are critical for a proper modeling of the Stokes profiles of spectral lines originating in the tenuous and highly dynamic plasmas of the chromosphere and transition region: quantum level population imbalance and interference (atomic polarization), frequency coherence effects in polarized resonance scattering (partial frequency redistribution), and the impact of arbitrary magnetic fields on the atomic polarization and the radiation field. We present first results of atmospheric and magnetic inversions, and discuss future developments for the project.

Keywords: Polarization - scattering - radiative transfer - solar atmosphere

1. INTRODUCTION

The solar chromosphere lies between the relatively cold, few thousand kelvin photosphere and the hot, million kelvin corona. This extended region spans about nine pressure scale heights and, even though it shows lower temperatures than the overlying corona, its larger density requires a comparatively larger energy deposit for its maintenance (e.g., [Carlsson et al. 2019](#)). The magnetic fields that permeate the solar atmosphere and dominate the structuring of the low- β plasma (where β is the ratio of gas to magnetic pressure) are key to understanding the coupling of its various layers and how the energy that is produced in the inner layers of the solar atmosphere is transported outward, and converted into heating of the chromosphere and corona. One of the main challenges of solar physics faced nowadays is the determination of the magnetic field in the upper solar atmosphere (e.g., the review by [Trujillo Bueno & del Pino Alemán 2022](#)). The polarization of the electromagnetic radiation emerging from the solar atmosphere carries information on the physical properties of the emitting plasma, including the magnetic field. Therefore, the study of the polarized solar spectrum is critical to uncovering the properties of the magnetic field, which in turn allows us to better understand the physical processes taking place in the solar atmosphere.

Stokes inversion techniques are a necessary tool to infer the physical properties of the solar plasma from spectropolarimetric observations. During the last decades, sophisticated Stokes inversion codes have been developed and applied to solar observations (see the reviews by [del Toro Iniesta & Ruiz Cobo 2016](#); [Lagg et al. 2017](#); [de la Cruz Rodríguez & van Noort 2017](#), and references therein), but there is still need for progress especially regarding the interpretation of spectropolarimetric profiles of chromospheric and coronal lines. As the plasma density decreases with height in the solar atmosphere, collisional processes become less and less important in determining the excitation and ionization balance of atoms, and spectral lines form outside of thermodynamical equilibrium (non-LTE). Moreover, photon coherence in scattering processes becomes increasingly important (the so called partial frequency redistribution, PRD), dramatically impacting polarized spectral line formation. While some of today's Stokes inversion codes can account for non-LTE effects (e.g., NICOLE, [Socas-Navarro et al. 2000, 2015](#), and SNAPi, [Milić & van Noort](#)

* Affiliate Scientist of the National Center for Atmospheric Research, Boulder, CO, USA.

2018) and even partial frequency redistribution (PRD) effects (STiC, [de la Cruz Rodríguez et al. 2019](#), and DeSIRE, [Ruiz Cobo et al. 2022](#)), these codes only account for Zeeman-effect polarization.

In the chromosphere, however, the excitation state of the atoms is affected by the anisotropy of the incident radiation and the atomic levels become polarized (through population imbalance and quantum coherence among the magnetic sublevels in the atom). This condition produces the so-called scattering polarization of the re-emitted radiation, which is sensitive to the magnetic field via the Hanle effect (e.g., [Trujillo Bueno 2001](#); [Landi Degl’Innocenti & Landolfi 2004](#)). There are both theoretical and numerical complexities implied by modeling atomic polarization, e.g., the necessity to keep track of the geometry with respect to the propagation directions of radiation within the atmosphere, instead of just the current line of sight (LOS), and to account for the breaking of axial symmetry in the pumping radiation field caused by horizontal radiation transfer, which is also a source of scattering polarization (e.g., [Manso Sainz & Trujillo Bueno 2011](#)). A well-known inversion code that includes some of these physical ingredients is HAZEL ([Asensio Ramos et al. 2008](#)), although its present treatment of radiation transfer (RT) is not applicable to the spectral lines originating in optically thick regions of the solar chromosphere. Moreover, it does not account for PRD effects.

Most of the inversion techniques accounting for RT and non-LTE rely on the computation of response functions ([Magain 1986](#); [Landi Degl’Innocenti & Landolfi 2004](#)). The response function can be computed numerically (e.g., NICOLE and STiC) or analytically (e.g., the SNAPi code). The former method is very time consuming, and it typically dominates the computing requirements of the inversion procedure. While the latter is theoretically much faster, its speed and performance have only been tested without atomic polarization. Moreover, the analytical calculation of response functions requires to explicitly account for all interdependencies in the statistical equilibrium (SE) equations. This is already a complex problem when only accounting for atomic populations ([Milić & van Noort 2017](#)) and the complexity dramatically increases when accounting for atomic polarization.

Recently, the sounding rocket experiments CLASP and CLASP2 have provided unprecedented spectropolarimetric observations of the H I Ly- α and the Mg II h and k lines, respectively ([Kano et al. 2017](#); [Ishikawa et al. 2021](#)). These observations have confirmed theoretical predictions based on the quantum theory of spectral line polarization ([Trujillo Bueno et al. 2011](#); [Belluzzi & Trujillo Bueno 2012](#); [Belluzzi et al. 2012](#); [Štěpán et al. 2015](#); [Alsina Ballester et al. 2016](#); [del Pino Alemán et al. 2016](#); [Manso Sainz et al. 2019](#); [del Pino Alemán et al. 2020](#)), showing clearly the impact of scattering polarization and the magneto-optical (MO) and PRD effects on the observed polarization profiles. The same observations have also revealed some surprises, which have expanded our understanding of the scattering polarization in strong resonance lines ([Trujillo Bueno et al. 2018](#)). It has thus become clear that there is a need for diagnostic tools that are capable of taking into account all these necessary physical ingredients to model the polarization of strong chromospheric spectral lines.

In this paper we present the Tenerife Inversion Code (TIC), which takes into account scattering polarization and the effects of PRD and quantum level interference in the presence of arbitrary magnetic fields (from zero field to the complete Paschen-Back regime). To achieve this, TIC is based on the HanleRT spectral synthesis code ([del Pino Alemán et al. 2016, 2020](#)). In § 2 we describe the inversion algorithm and its implementation. In § 3 we show the application of the TIC to spectral profiles obtained from the synthesis in semi-empirical one-dimensional models in order to assess its performance in this necessary but non-trivial test. We show applications both without and with added photon noise. We finish this section with an application relying only on the circular polarization profiles. Finally, we present our summary and discussion in § 4, including a brief discussion on future developments for the project.

2. INVERSION CODE

We call inversion the semi-automatic or automatic process of inferring the magnetized model atmosphere that, when input into its spectral synthesis module (hereafter, forward engine), gives the best fit to a given observation. Of course, the inference is highly dependent on the forward engine and how well it describes the physics of the generation and transfer of polarized radiation. In this section we describe the main characteristics of the TIC, a numerical code for the inversion of Stokes profiles that takes into account the physical mechanisms necessary for the modeling of the polarization in strong resonance chromospheric spectral lines, namely, atomic polarization and PRD effects in the presence of magnetic fields of arbitrary strength. TIC relies on HanleRT ([del Pino Alemán et al. 2016, 2020](#)) as its forward engine.

2.1. Forward synthesis module

HanleRT was developed by [del Pino Alemán et al. \(2016, 2020\)](#) to solve the problem of the generation and transfer of polarized radiation out of local thermodynamical equilibrium (non-LTE) in one-dimensional plane-parallel atmospheric models, taking into account the coherent scattering of radiation by polarized multi-term atoms in arbitrary magnetic fields ([Casini et al. 2014, 2017a,b](#)). Consequently, the TIC can take into account scattering polarization with PRD effects, and quantum level interference, for arbitrary magnetic fields. Even though HanleRT implements the general angle-dependent redistribution function to describe PRD effects, in this paper we show results obtained with the angle-averaged approximation ([Mihalas 1970; Belluzzi & Trujillo Bueno 2014](#)) in order to significantly reduce the total computational cost.

2.2. Inversion module

As any inversion code, the TIC finds the model atmosphere that produces the best fit to a given set of Stokes profiles via its forward engine. To this end, the inversion code determines at each iteration step how the physical parameters describing the current model atmosphere must be modified in order to improve the fit. The magnitude of these changes is determined from the response functions (e.g., [Magain 1986; Landi Degl’Innocenti & Landolfi 2004; Uitenbroek 2006](#)) of the emergent Stokes profiles to perturbations in the physical parameters of the model in a set of chosen nodes sampling the atmosphere’s height stratification. This is the usual strategy employed by existing inversion codes.

The physical parameters of the model atmosphere used in the TIC are the plasma temperature (T), the bulk velocity vector (\mathbf{v}), the micro-turbulent velocity (v_{turb}), the magnetic field vector (\mathbf{B}), and the gas pressure at the top boundary¹ (P). In the spectral synthesis code, the number densities of the different atomic species are computed by solving the equation of state with the method of [Wittmann \(1974\)](#).

Usually, inversion codes retrieve the atmospheric stratification along the LOS and, in particular, the bulk velocity along the same direction. However, when accounting for scattering polarization, the orientation of the LOS with respect to the atmospheric structure becomes important. Therefore, even in a one-dimensional (1D) plane-parallel model atmosphere, we must distinguish between the vertical and LOS directions in the inversion. Although we can include the three components of the macroscopic velocity vector, its horizontal component is a source of scattering polarization due to the breaking of axial symmetry (e.g., [Štěpán & Trujillo Bueno 2016; del Pino Alemán et al. 2018; Jaume Bestard et al. 2021](#)). Because the inversions in this paper are performed using Stokes profiles calculated in known axially symmetric model atmospheres, we assume that the horizontal component of the velocity field is zero, preserving the axial symmetry, and we only invert its vertical component.

In order to find the best fit to a given set of Stokes profiles, we minimize a cost function that accounts for both the difference between the data and the synthetic profiles emerging from the inverted model, and additional constraints imposed on the solution (regularizations). The cost function can thus be written as

$$\chi^2 = \frac{1}{4N_\lambda} \sum_{i=1}^4 \sum_{j=1}^{N_\lambda} \left[\frac{I_i^{\text{obs}}(\lambda_j) - I_i^{\text{syn}}(\lambda_j)}{\sigma_i(\lambda_j)} \right]^2 w_i^2 + \sum_{n=1}^N \alpha_n r_n^2(p), \quad (1)$$

where N_λ is the number of wavelength points in the observed Stokes profiles. $I_i^{\text{obs}}(\lambda_j)$ and $I_i^{\text{syn}}(\lambda_j)$ are the i -th Stokes parameters ($i = I, Q, U, \text{ and } V$) at each j -th wavelength position for the observed and synthetic profile, respectively. $\sigma_i(\lambda_j)$ is the noise of each “ i ” Stokes parameter in the observation, assumed to be Gaussian and, in general, dependent on the wavelength index “ j ”. w_i is a weight for each Stokes parameter to account for the expected difference in their order of magnitude for different physical scenarios.² $r_n(p)$ is a regularization function weighted by α_n . These regularization functions include penalties on the first derivatives of the stratification of the model parameters (bulk velocity, micro-turbulent velocity, and magnetic field, favoring smooth stratifications over complex ones), penalties on the second derivatives of the stratification of the model parameters (temperature, favoring smooth gradients over complex ones), and penalties on deviations from a given value for a model parameter (gas pressure at the top boundary, favoring solutions fulfilling some a priori knowledge). These regularization functions have been used in other inversion codes such as the STiC ([de la Cruz Rodríguez et al. 2019](#)). The regularization function weights α_n are not kept constant during the inversion. At the beginning of the inversion procedure, when χ^2 can be several orders

¹ In order to derive the model’s density stratification, we assume hydrostatic equilibrium (e.g., [Mihalas 1970](#)), reason why only the boundary value is needed once the temperature stratification is known.

² Note that the intensity in solar spectral lines is usually at least two orders of magnitude larger than the polarization signals and it would thus dominate the cost function if no weights were added.

of magnitude larger than the target value, we start with enhanced values of α_n , such that the regularization term in Eq. (1) is of the same order of magnitude as the first term describing just the quality of the fit. As the inversion moves toward smaller χ^2 , the regularization function weights are progressively reduced until they reach the values that are specified for the inversion solution.

We have implemented the Levenberg-Marquardt algorithm (Press et al. 2007) to minimize the cost function in Eq. (1), with the Hessian matrix approximated by only using the first derivatives with respect to the model parameters (i.e. the response functions). The Hessian being second order, we approximate the second derivatives with the product of first derivatives. We thus compute the response functions of all model parameters at each iteration step. To that end, we perturb their node values and recompute the Stokes profiles to compare them with the ones resulting from the unperturbed model. We have implemented the calculation of these response functions with both central differences (compute the Stokes parameters perturbing both positively and negatively each parameter) and forward differences (compute the Stokes parameter perturbing each parameter only once). Although the former is more accurate, we have not found significant differences between the response functions retrieved by the two methods in our tests, and thus we apply the latter throughout this paper as it requires half the number of forward syntheses.

Regarding the damping parameter λ of the Levenberg-Marquardt algorithm (see Press et al. 2007), we have implemented a parabolic interpolation in order to optimize its value at each iteration. This procedure, dubbed *backtracking* method, is adopted also by other inversion codes, such as the STiC and HAZEL.

In order to determine the correction to the model parameters we need to solve a linear system of equations. We apply the modified singular value decomposition (SVD) method proposed by Ruiz Cobo & del Toro Iniesta (1992). We start the SVD with a relatively small (10^{-6}) tolerance factor ϵ and check the resulting corrections. If they are larger than a certain threshold (e.g., the correction to the temperature is larger than $4 \cdot 10^3$ K or the correction to the velocity is larger than 10 km/s), we increase the tolerance factor and solve the system again, repeating the procedure until the corrections comply with the pre-established threshold or ϵ is of order 10^{-3} .

The uncertainties in the inverted model parameters could also be estimated by applying Bayes' theorem with a Monte Carlo method. However, the computational cost of each forward solution makes this approach unfeasible. We thus estimate the uncertainties following the approach by Sánchez Almeida (1997) (see also del Toro Iniesta 2003) to compute the variance of each model parameter at each node (p):

$$\sigma_p^2 = \frac{2\Delta\chi^2}{N_{\text{nodes}}} H^{-1}, \quad (2)$$

where N_{nodes} is the number of nodes, $\Delta\chi^2$ is the first term in the right side of Eq. (1), i.e., the χ^2 without the regularization term, and H^{-1} is the inverse matrix of the Hessian matrix. H^{-1} is simply approximated by the inverse diagonal elements of H . Since these diagonal elements are in fact the squares of the response functions, the uncertainties can thus be estimated directly from the values of the response functions, giving an immediate estimation of how well the inferred parameters are constrained. Even though this approach does not give accurate uncertainties, it provides an idea of the sensitivity of the different physical parameters to the changes in each of the nodes in the model atmosphere.

3. INVERSION OF THEORETICAL MG II h & k PROFILES

We have chosen to test the inversion code with the Mg II h and k doublet around 279 nm. This decision is not only motivated by the physical properties of this doublet, namely, the significance of non-LTE, PRD and scattering polarization effects in these lines, but also because of the successful observations by the CLASP2 and CLASP2.1 missions, whose interpretation would greatly benefit from the availability of a suitable inversion method. To mimic the real resolution of observations, we adopted the spectral sampling of the IRIS instrument (De Pontieu et al. 2014) for the line cores of the synthetic profiles, that is, 25.4 mÅ/pixel, whereas for the line wings the sampling is 8 times larger. In the forward calculation a thinner wavelength grid is generated to synthesize the profiles with sufficient accuracy.

The Stokes profiles of the Mg II h and k lines can be reliably modeled by solving the problem of the generation and transfer of polarized radiation using a two-term Mg II atomic model (including the ground level of Mg II, the first excited term of Mg II with the two upper levels of the h and k transition, as well as the ground term of Mg III), as can be easily checked by comparing the two-term results of del Pino Alemán et al. (2016) with the three-term results of del Pino Alemán et al. (2020). Therefore, in this paper we have used a two-term atomic model taking into account the effects of PRD, quantum interference, and the impact of arbitrary magnetic fields (see the cited papers for further details on the spectral synthesis).

In this section we show the capability of the TIC to retrieve a known model atmosphere by inverting a set of synthetic Stokes parameters. First, we apply the inversion code directly to the Stokes profiles resulting from the synthesis, and later, in §. 3.3, we perform the inversion after adding Gaussian noise to them.

When modeling RT with scattering polarization, PRD effects, and with arbitrary magnetic fields, the inversion becomes very time consuming. In particular, inverting the whole set of physical parameters at the same time becomes prohibitive.

In this paper, the full inversions are broken down into six cycles. In the first two cycles (hereafter, the *Stokes-I inversion*) we only fit the Stokes I profile by inverting the temperature, micro-turbulent velocity, bulk vertical velocity (v_{ver}), and the top boundary gas pressure (using 8, 3, 4, and 1 nodes, respectively). It has been shown (de la Cruz Rodríguez et al. 2016, 2019; Sainz Dalda et al. 2019) that it is possible to recover the thermal stratification of the model atmosphere by only fitting the intensity profile of the Mg II h and k lines. We then fix these non-magnetic model parameters and only invert the magnetic field vector in the subsequent four cycles (hereafter, the *magnetic inversion*). This separation between Stokes- I and magnetic inversions is often possible because, for solar applications, both the magnetic field and the anisotropy are small enough (relative to the Doppler width and the mean radiation field, respectively) as to typically have a negligible impact on the Stokes I profile of these spectral lines. In our tests, the magnetic field is described by the longitudinal component B_{\parallel} , the transverse component B_{\perp} , and the azimuth on the plane of sky ϕ_B .

The physical model of scattering polarization considered in this work is highly multi-dimensional, and the inversion can easily get trapped in a local minimum. In order to prevent this, we first fit the circular polarization (usually dominated by the Zeeman effect) to retrieve B_{\parallel} in the first two magnetic cycles. Doing it in two cycles allows us to retrieve a smooth stratification. As the circular polarization is only sensitive to the magnetic field in the chromosphere, its value at the upper and lower boundaries of the height domain cannot be well constrained in these cycles. The retrieved two-node model is a suitable and smooth initialization for the second cycle. Even with this strategy the third cycle, the most important in the inversion process, can still get stuck in a local minimum. If the χ^2 is not significantly reduced, this cycle must be restarted with different initial values for B_{\perp} and ϕ_B . The last cycle then improves the fit to the Stokes profiles by allowing more freedom in the stratification. The four cycles of the magnetic field inversion are thus performed as follows:

1. 2 nodes in B_{\parallel} to fit only the Stokes V profile.
2. Starting from cycle 1, 4 nodes in B_{\parallel} to fit only the Stokes V parameter.
3. Starting from cycle 2, 4 nodes in B_{\parallel} , 1 node in B_{\perp} , and 1 node in ϕ_B to fit Stokes Q and U , and V , with relatively small weights for the linear polarization.
4. Starting from cycle 3, 4 nodes in B_{\parallel} , 4 nodes in B_{\perp} , and 1 node in ϕ_B to fit Stokes Q , U , and V , with larger weights for the linear polarization.

Following this inversion strategy, each full inversion (i.e. 6 cycles) shown in this section takes of the order of 10^3 CPU hours (@2.10GHz). We have tested adding one more cycle including all physical parameters together, but the result is not significantly improved and the required computing time is tripled.

We tested the TIC code with the Mg II h and k Stokes profiles in two different magnetic regimes: the Hanle effect around the regime of criticality, and in the “saturation limit”. In the former, the magnetic field produces Zeeman splittings of the order of the line’s natural width. In the latter, the magnetic field is sufficiently strong to completely relax the quantum coherence between magnetic sublevels, and the line’s scattering polarization becomes only sensitive to the direction of the magnetic field, but not to its strength. The critical magnetic field for the onset of the Hanle effect in the Mg II k line is ~ 22 G (remember that the h line is intrinsically non polarizable through atomic alignment due to the angular momentum $J = 1/2$ of both lower and upper levels). Therefore, the linear polarization in the Mg II k line is sensitive via the Hanle effect to magnetic field strengths between ~ 5 and ~ 100 G. In §. 3.1, where we test the Hanle regime, the chosen magnetic field strength is within such limits. In Sect. 3.2, where we test the saturated Hanle regime, the chosen magnetic field strength is larger than 100 G.

3.1. Hanle effect regime

In the tests shown in this section we impose a magnetic field in the Hanle regime for the Mg II k line, that is, between ~ 5 and ~ 100 G. We want to emphasize that for magnetic field strengths outside of this range (but still

not large enough to produce significant linear polarization via the Zeeman effect) the linear polarization is completely insensitive to the magnetic field strength and the inversion cannot possibly recover its value.

For our model atmosphere, we have taken the temperature, micro-turbulent velocity, and electron number density of model C of Fontenla et al. (1993, hereafter, FAL-C model, see red circles in panels (c), (e), and (f) of Fig. 1, respectively). We have added a smooth stratification of the bulk vertical velocity (see red circles in panel (d) of Fig. 1), and an assigned stratification of the magnetic field vector (red circles in the right column panels of Fig. 2).

As explained above, we first invert the temperature, the micro-turbulent and bulk vertical velocities, and the gas pressure at the top boundary by fitting just the Stokes I profile. The inversion is initialized with the temperature and micro-turbulent velocity from the model P of Fontenla et al. (1993, hereafter, FAL-P model). The result of this inversion is shown in Fig. 1. Panel (a) shows the theoretical profile that represents our observation (red circles) and the fit resulting from the inversion (black solid curve). The stratification of the temperature (panel (c)), the bulk vertical velocity (panel (d)), the micro-turbulent velocity (panel (e)), and the electron density (panel (f)) are shown for the original model (red circles) and the inverted model (black solid curve). The green “+” symbols in panels (c)-(e) of Fig. 1 indicate the inversion nodes and the vertical black solid bars represent the uncertainty derived from the response function following Eq. (2). The black dotted curves in panels (c)-(f) show the height where the optical depth τ_λ for each wavelength is equal to unity (right vertical axis in each panel).

This Stokes- I inversion test was performed for a LOS with $\mu = 0.3$, where μ is the cosine of the heliocentric angle. The inversion successfully fits the theoretical profiles and recovers the main features of the original model atmosphere above $\log_{10}(\tau_{500}) = -3$ (note that the Mg II lines are insensitive to the model parameters at larger optical depths).

The Hanle effect is the modification of the scattering polarization at line center in the presence of a magnetic field. Therefore, it is important to check if the inverted atmosphere is able to reproduce the zero-field scattering polarization signals. The red dashed curves in panel (b) of Fig. 1 show the Stokes Q (bottom curves) and Q/I (top curves) profiles synthesized in the original model. Likewise, the black solid curves in the same panel show the Stokes Q and Q/I profiles synthesized in the inverted model. The Stokes Q profile is reasonably well fitted, except for slight differences in the center (k_3) and the wings (k_1) of the k line. However, the comparison is worse if we look at the fractional linear polarization Q/I instead. Because the intensity around the k_1 minimum is relatively small, the differences in Q/I are amplified in this spectral region.

In panel (c) of Fig. 1 we see that in the range $\log_{10}(\tau_{500}) = -6$ to -8 the inverted temperature is not exactly that of the original model. However, the Q profiles synthesized in the original and recovered models are almost the same. Therefore, either the sensitivity to the temperature at those heights of the atmosphere is rather small, or the temperature is to some degree degenerate with the electron density or the micro-turbulent velocity. Nevertheless, it is important to emphasize that the behavior of the radiation field (and in particular its anisotropy) seems to be recovered from the Stokes- I inversion, which allows us to successively invert the magnetic field vector while fixing the rest of atmospheric parameters. We remind the reader that the results shown here correspond to an axially symmetric problem and thus represent an idealized case. In the general non-axially symmetric case, we should not expect the atmospheric model inverted with just the intensity to reproduce the polarization profiles of the actual atmosphere, even in the absence of a magnetic field.

We now perform the magnetic field inversion in four cycles as described above. The initial values are 0 G, 10 G, and 28.6° (0.5 radians) for the longitudinal magnetic field, the transverse magnetic field, and the azimuth, respectively. In panels (a)-(c) of Fig. 2 we show the original (red circles) and fitted (black solid curves) polarization profiles. The panels in the right column of Fig. 2 show the longitudinal component of the magnetic field (panel (d)), the transverse component of the magnetic field (panel (e)), and the magnetic field azimuth (panel (f)) for the original (red circles) and the inverted (black solid curves) models, as well as the absolute difference Δ between them (blue dashed curves and the right vertical axes).

The longitudinal component of the magnetic field is mostly constrained by the Stokes V parameter via the Zeeman effect (from $\log_{10}(\tau_{500}) \approx -4.5$ and above) and the MO effects in the Stokes Q and U wings (in the range $\log_{10}(\tau_{500}) \approx -3$ to ≈ -5). Between $\log_{10}(\tau_{500}) \approx -7$ and ≈ -4 the absolute error Δ on the longitudinal magnetic field component is at most 3 G. The transverse component of the magnetic field is determined with an error smaller than 12 G above $\log_{10}(\tau_{500}) \approx -5$. The linear polarization in the k line core (k_3) is only modified by the Hanle effect, while the troughs (k_2 and h_2) are modified by both the Hanle and the MO effects, the latter usually being more significant. Consequently, the transverse component is best determined at around $\log_{10}(\tau_{500}) \approx -6.5$. Finally, the inverted magnetic field azimuth differs from the original by less than 10° .

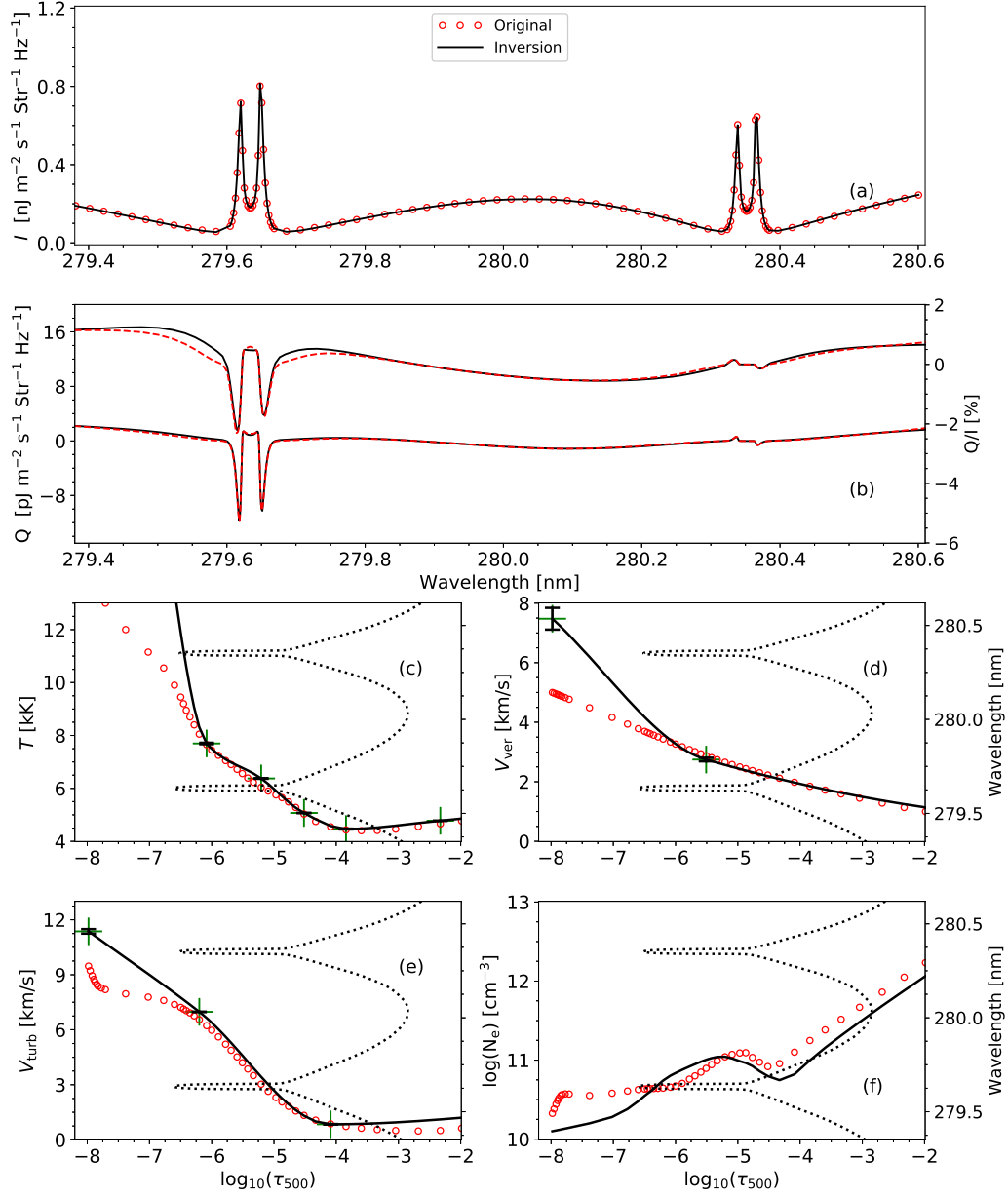


Figure 1. Stokes- I inversion of Mg II h and k line profiles calculated in the FAL-C model with a magnetic field in the Hanle regime. (a) Theoretical (red circles) and fitted (solid black curve) intensity profiles. (b) linear polarization Q (bottom curves) and fractional linear polarization Q/I (top curves) synthesized in the original unmagnetized model atmosphere (dashed red curves) and in the inverted atmosphere (solid black curves), for a LOS with $\mu = 0.3$. (c) Temperature, (d) bulk vertical velocity, (e) micro-turbulent velocity, and (f) electron density for the original (red dots) and inverted (solid black curve) atmosphere. The black dotted curves show the optical depth ($\log_{10}(\tau_{500})$) where $\tau = 1$ at each wavelength.

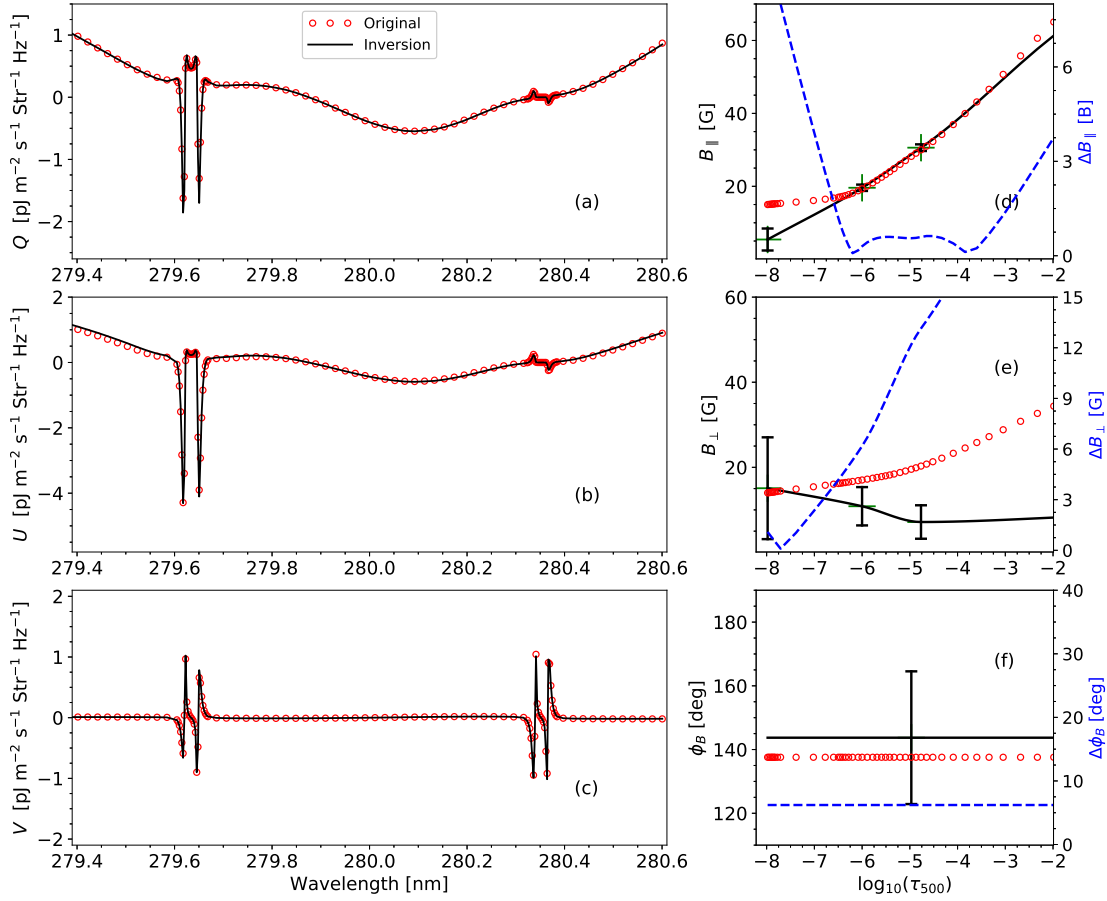


Figure 2. Magnetic inversion of Mg II h and k line profiles calculated in the FAL-C model with a magnetic field in the Hanle regime. Linear polarization Q (a) and U (b), and circular polarization V (c) profiles for the theoretical (red circles) and fitted (black solid curves) profiles for a LOS with $\mu = 0.3$. Longitudinal magnetic field (d), transverse magnetic field (e), and magnetic field azimuth (f) for the original (red circles) and inverted (black solid curves) model atmosphere. The absolute differences between the original and inverted stratifications are shown by the blue dashed curves and they correspond to the scales on the right vertical axis.

It is obvious that the inversion does not retrieve the original magnetic field exactly, and it just finds the solution that best fits the Stokes profiles. Given the errors on the temperature and density of the inverted model, it can be expected that the ensuing changes in the radiation field and formation height of the lines will also impact the determination of the magnetic field. This can result in errors such as those in Fig. 2. Nonetheless, the inferred magnetic field provides a reasonably good estimation of the original magnetic field.

We repeated the same test for a LOS with $\mu = 0.8$. The results of this inversion are shown in Fig. 3. The LOS for this test is much closer to the disk center, which usually implies a weaker linear scattering polarization. In fact, the Stokes Q and U parameters are approximately a factor 4 smaller in the line wings and about a factor 2 smaller at the troughs. The weak signals of the linear polarization result in a significant decrease of the accuracy in the determination of the transverse magnetic field (the inferred azimuth is 40° away from the actual value). However, the longitudinal component of the magnetic field is constrained by the Zeeman and MO effects and thus is equally well determined between $\log_{10}(\tau_{500}) \approx -3$ and ≈ -7 . Note that, for a LOS with $\mu = 0.8$, the spectrum is formed deeper in the atmosphere.

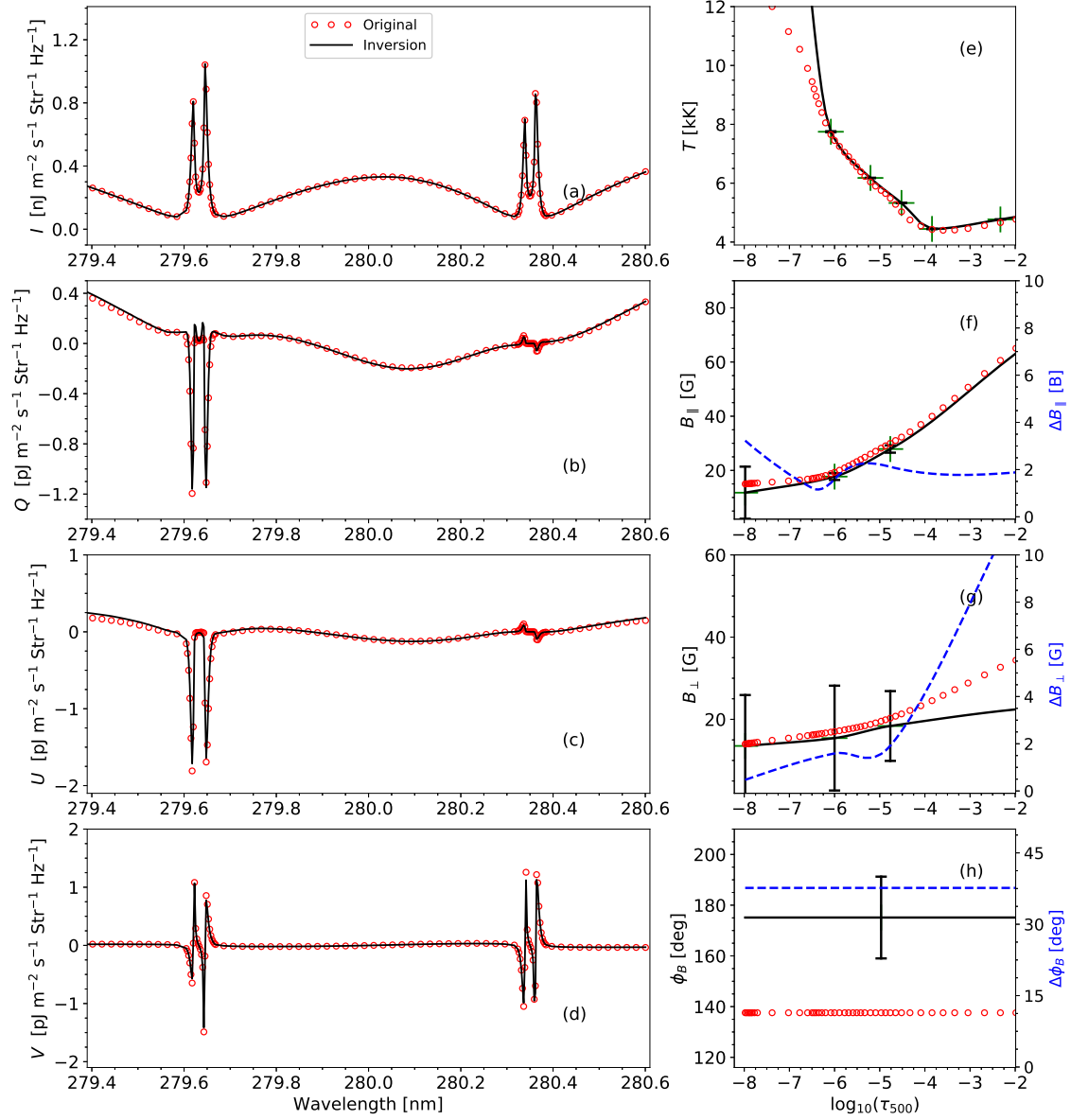


Figure 3. Magnetic inversion of Stokes profiles calculated in the FAL-C model with a magnetic field in the Hanle regime. Same as Fig. 2, but for a LOS with $\mu = 0.8$. Here we have added panels to show the Stokes I fit (a) as well as the inversion of the temperature (e).

3.2. Saturated Hanle effect regime

In the tests shown in this section we impose a magnetic field corresponding to the saturated Hanle regime of the Mg II k line, that is, larger than ~ 100 G. In this regime the linear scattering polarization at the core of the k line is no longer sensitive to the magnetic field strength, but only to its direction. Therefore, in this situation, the only constraint to the magnetic field strength comes from the Zeeman and the MO effects.

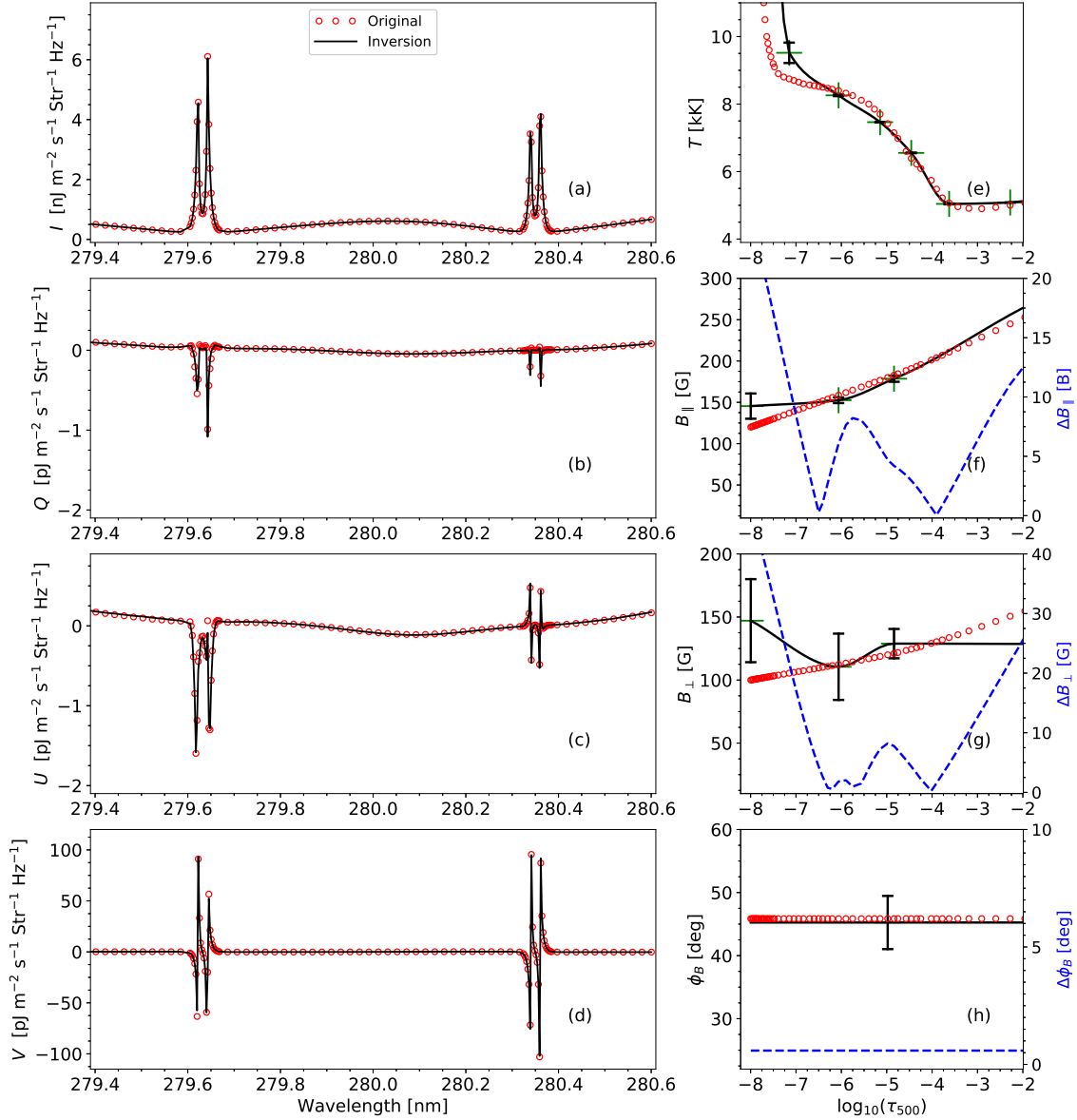


Figure 4. Magnetic inversion of Stokes profiles calculated in the FAL-P model for a line of sight with $\mu = 0.8$. Same as Fig. 3, but for the modified FAL-P model in the presence of a stronger magnetic field in the Hanle saturation regime.

Because we are imposing a stronger magnetic field, we perform this test not only for the FAL-C model, but also for the FAL-P model, as it should be more representative of plage regions where we can find magnetic fields with such strengths. Similarly to what we did for the FAL-C model, we added a smooth stratification of the bulk vertical velocity, as well as a given stratification of the magnetic field vector (red dots in panels (e)-(h) of Fig. 4). The inversion for the FAL-P model is initialized with the temperature and micro-turbulent velocity of the FAL-C model.

We follow the same inversion procedure as in § 3.1, namely, a non-magnetic inversion followed by four cycles where only the magnetic field vector is inverted. We tried using the same initialization for the magnetic field as in the former

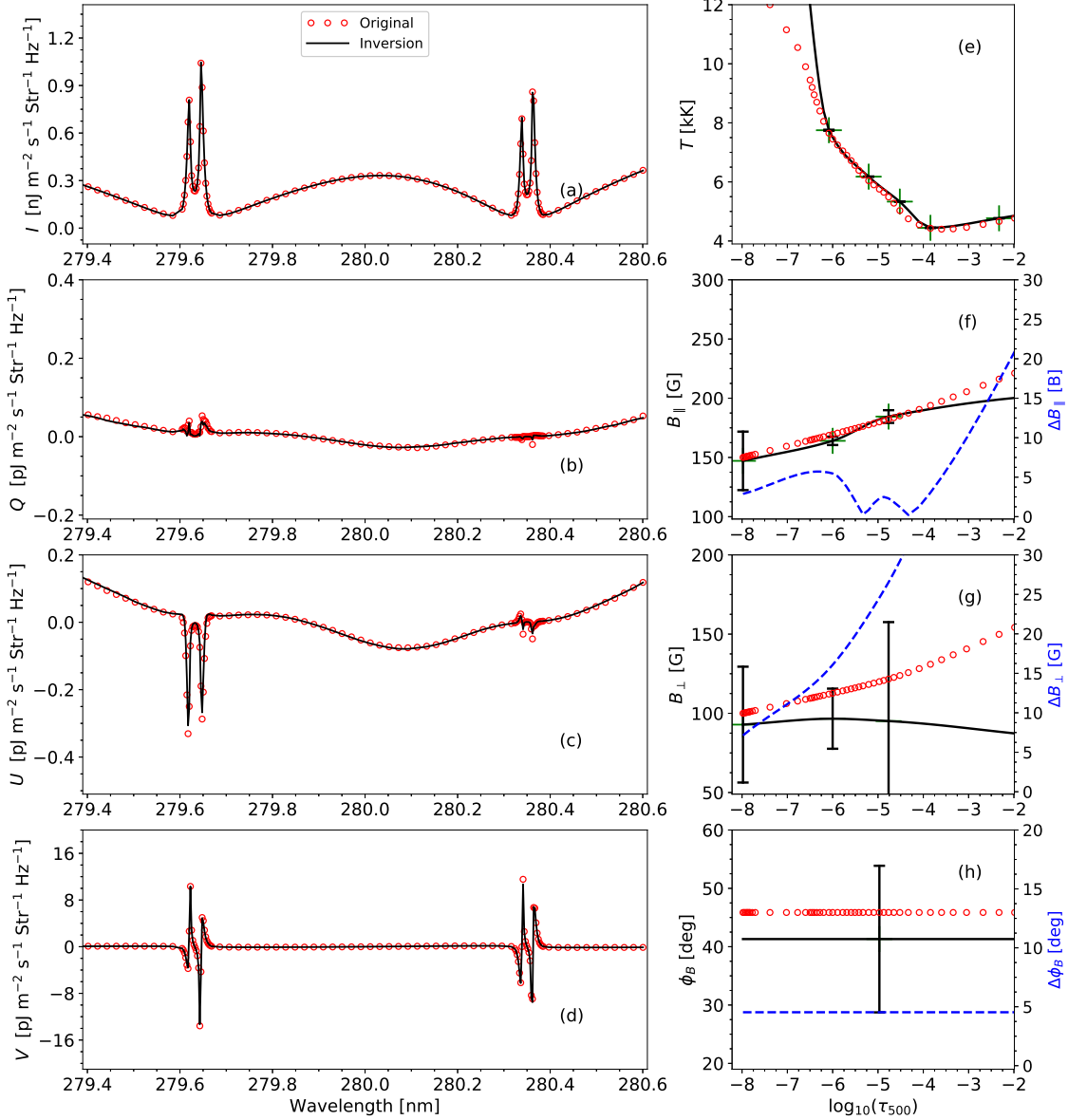


Figure 5. Magnetic inversion of Stokes profiles calculated in the FAL-C model for a line of sight with $\mu = 0.8$. Same as Fig. 3, but with a stronger magnetic field in the Hanle saturation regime.

test. However, for the FAL-C model, the initial transverse magnetic field had to be increased from 10 to 60 G to reach convergence in the inversion process. As seen in Fig. 4, the fractional linear polarization is relatively weak, which affects the calculation of the response function. For example, for $B_{\perp} = 10$ G the difference between two syntheses for a small perturbation in the magnetic field is of the order of the accuracy of the forward engine. In Figs. 4 and 5 we show the inversion results for the FAL-P and FAL-C models, respectively. In both models, the inversion code does a good job at retrieving the longitudinal component of the magnetic field in the region where the near wings of the Mg II resonance lines are formed (between $\log_{10}(\tau_{500}) \approx -4$ to ≈ -6), constrained by both the circular polarization

caused by the Zeeman effect and the linear polarization in the wings sensitive to the MO effects. The inversion of the transverse component of the magnetic field relies mostly on the Hanle effect in the core of the k line, and in the FAL-P model it is relatively well determined between $\log_{10}(\tau_{500}) \approx -5.0$ and ≈ -6.5 . It is also worth mentioning that we needed to significantly increase the weights in the cost function (Eq. (1)) for the linear polarization in this inversion due to the relative amplitudes of the Stokes parameters. Otherwise, the linear polarization is not well fitted and the transverse magnetic field cannot be constrained.

3.3. Noisy Profiles

In the previous sections we have only considered theoretical Stokes profiles free of noise. In this section we repeat the test of § 3.1 (Hanle regime, FAL-C model, for a LOS with $\mu = 0.3$) but adding random noise to the synthetic profiles. The added noise follows a Gaussian distribution with a standard deviation of $\sigma = 0.2$ [pJ m⁻² s⁻¹ Str⁻¹ Hz⁻¹]. This corresponds to a polarimetric noise slightly larger than 10^{-3} in the line wings, but better than 10^{-3} in the line core. This condition is comparable to that of the plaque target of the CLASP2 mission (Ishikawa et al. 2021).

With this level of noise, the wing structures in the linear polarization profiles are still preserved. Instead, the antisymmetric linear polarization feature around the h line core is lost in the noise. We invert these profiles with the same strategy described above and show the results in Fig. 6. A comparison with the results from Fig. 2, also shown in Fig. 6, indicates that, between $\log_{10}(\tau_{500}) \approx -5$ and -6 , the inferred longitudinal magnetic field is almost the same as in the noise-free tests. We note how, despite the poorer precision of the inversion, leading to larger parameter uncertainties, the inferred solution “in the mean” is still rather accurately matching the original model.

The results of our tests are very promising in view of the possible application of TIC to the interpretation of data from the recent the CLASP2 and CLASP2.1 missions.

3.4. Longitudinal Magnetic Field

The circular polarization is mainly produced by the Zeeman effect and it is only sensitive to the longitudinal component of the magnetic field. However, due to PRD effects, scattering polarization has a significant influence on the outer lobes of the Mg II h and k circular polarization profiles (Alsina Ballester et al. 2016; del Pino Alemán et al. 2016).

In this section we study the impact of neglecting atomic polarization in the inversion of the longitudinal component of the magnetic field. To this end, we carry out two inversions in which we only consider the Stokes I and V parameters, using a FAL-C model with an imposed magnetic field for a LOS with $\mu = 1$. For this test we fix the thermodynamic stratification and we only invert for the longitudinal component of the magnetic field. For the first inversion, we completely neglect scattering polarization in the synthesis of the circular polarization profile. For the second inversion, we include all physical ingredients as for the other tests in this paper. We find that the recovered longitudinal magnetic field is significantly overestimated when neglecting the anisotropy of the radiation field (see panel (c) in Fig. 7). This overestimation occurs mainly below $\log_{10}(\tau_{500}) \approx -5.5$, in the region where the outer lobes of the V profile are formed. At $\log_{10}(\tau_{500}) \approx -5.2$, the difference between the original and inverted magnetic field can reach ~ 24 G (≈ 12 % relative difference). When atomic polarization and the radiation field anisotropy are included, the inferred magnetic field is much closer to the original stratification at those heights where the emergent Stokes V is sensitive to the magnetic field.

The black curves in the left and middle panels in Fig. 7 show the synthetic profiles for the same atmospheric and magnetic field models accounting for the Zeeman effect without atomic polarization. It is clear that, when neglecting the scattering polarization, the outer lobes of the Stokes V profile are underestimated. Therefore, the inversion needs to increase the field strength in the lower atmosphere in order to compensate for this effect and fit the outer lobes.

4. SUMMARY AND DISCUSSIONS

In this paper we have presented the Tenerife Inversion Code, TIC, and tested it on synthetic spectropolarimetric profiles to infer the magnetic and thermodynamic structure of solar model atmospheres. TIC is based on the HanleRT forward synthesis engine, and takes into account all the physical mechanisms that are essential to the modeling of strong resonance spectral lines formed in the chromosphere and transition region: atomic polarization, magnetic field of arbitrary strength, and PRD effects. TIC minimizes a cost function measuring the quality of the fit to the Stokes data, and includes a series of regularization terms to additionally constrain the solution of this notoriously ill-posed inversion problem.

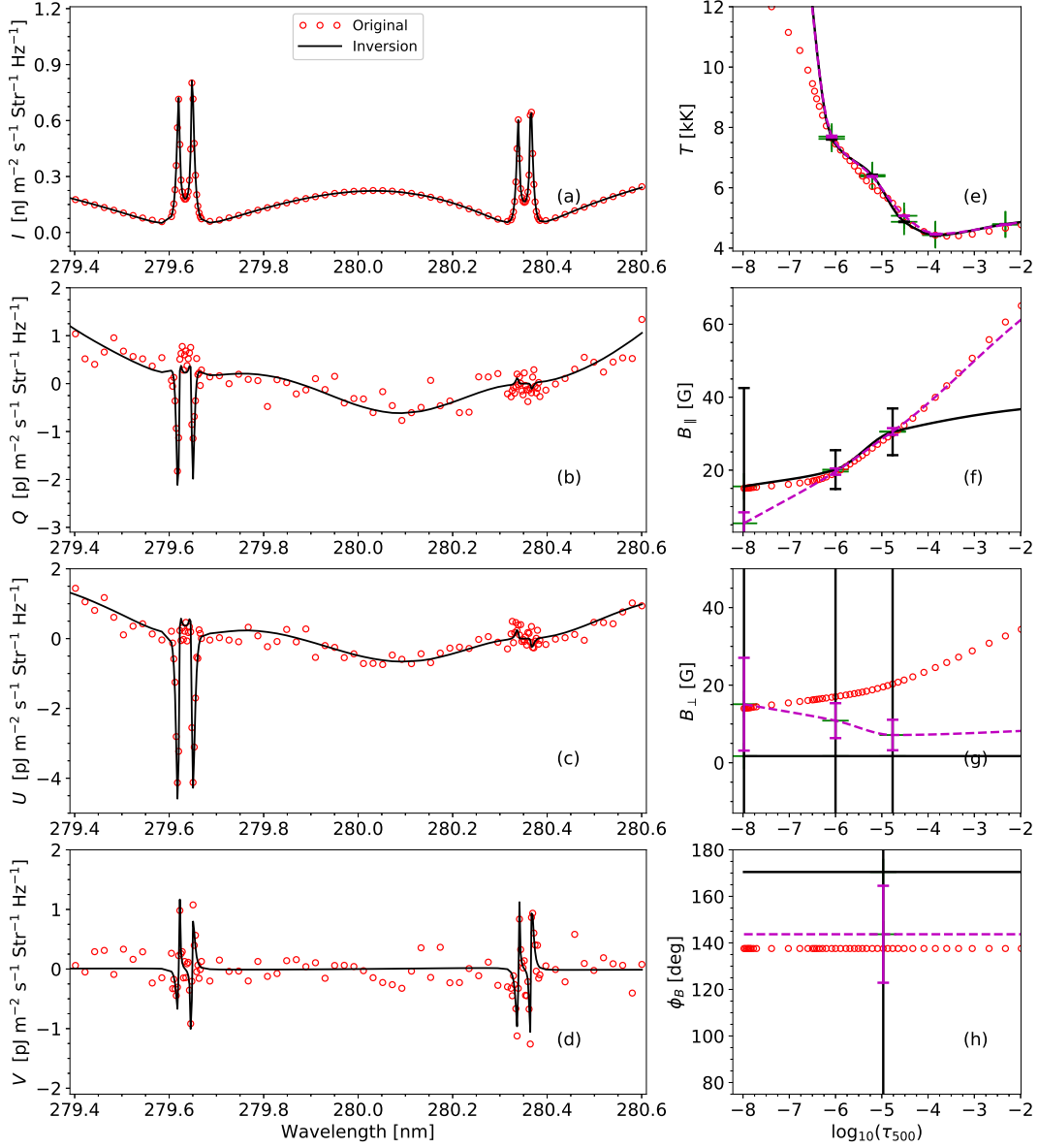


Figure 6. Magnetic inversion of Stokes profiles calculated in the FAL-C model with a magnetic field in the Hanle regime. Same than Fig. 2, but with gaussian noise (see text) added to the profiles. Here we have added panels to show the Stokes I fit (a) as well as the inversion of the temperature (e). The magenta curves show the inverted model from Fig. 2, that is, in the noise-free case.

To test the inversion code, we considered a modified version of the C and P models of Fontenla et al. (1993) to which we added a stratified bulk vertical velocity and a magnetic field. With these models, we computed the emergent Stokes profiles of the Mg II h and k lines for two different LOS. In particular, we performed tests for two relevant regimes of the magnetic field strength.

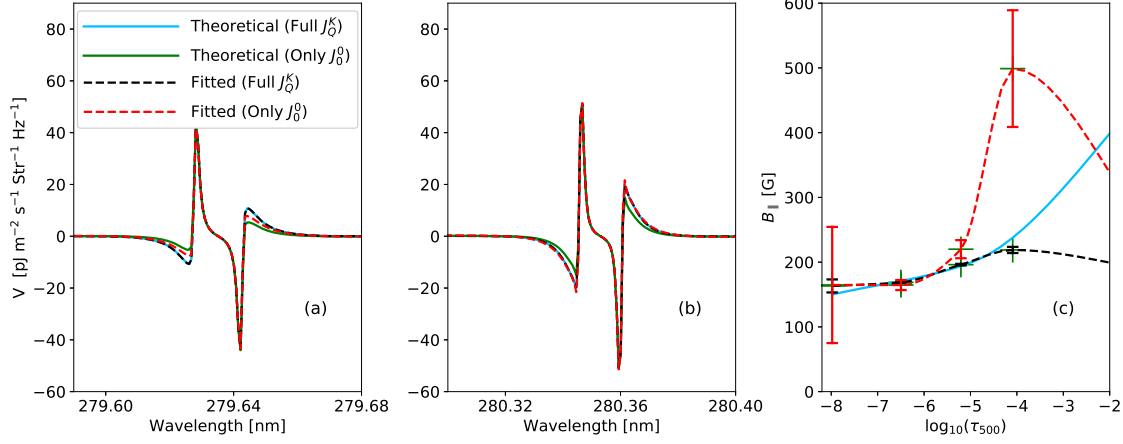


Figure 7. Theoretical (solid curves) and the fit (dashed curves) Stokes V profiles of the Mg II k (a) and h (b) lines. (c) input and inverted magnetic field model. The different colors represent different cases indicated in the legend, with “Full J_Q^0 ” and “Only J_Q^0 ” indicating that scattering polarization has been taking into account and neglected, respectively.

In the first test the magnetic field strength corresponds to the Hanle regime for the Mg II k line (the h line is intrinsically unpolarizable because the angular momentum of its upper and lower levels is 1/2 and thus it is not sensitive to the Hanle effect). In this regime, the Zeeman splitting is of the order of the natural width of the line, and the scattering polarization is sensitive to both the strength and direction of the magnetic field. In the second test the magnetic field strength is in the “saturated” Hanle regime. Here, the Zeeman splitting is at least one order of magnitude larger than the natural width of the line, and the scattering polarization is only sensitive to the direction of the magnetic field. The magnetic field strength chosen for the second test is such that the transverse Zeeman effect is still completely negligible.

We tested the performance of the inversion with and without photon noise and quantified how the inference of the stratification of physical parameters is affected by the increased uncertainty.

We proposed an inversion strategy that we applied to every test shown in this paper. This strategy follows the usual approach of first inferring only the stratification of the thermodynamic parameters (every physical parameter but the magnetic field) from just the intensity profile, and then invert the magnetic field with all four Stokes profiles after fixing the rest of the physical parameters. The inference of the transverse magnetic field component from the linear polarization profiles can be difficult, depending on the strength and direction of the field, and thus the inversion is iterated through several cycles in which we incrementally converge to the final solution. We determined a good working strategy using four magnetic inversion cycles. The convenience of performing the magnetic field inference in this way is twofold. On the one hand, by increasing the number of nodes and the weights for the linear polarization in incremental steps, always using the output of the previous step as an initial condition, we approach more stably the minimum of the cost function in Eq. (1). We have found that performing just one magnetic cycle can easily lead the inversion towards a local minimum of the cost function. On the other hand, the computing time is proportional to the number of nodes. By finding first a rough approximation to the final solution with fewer nodes, and then successively refine the result, we can reach the same or a better solution in significantly less time. While the inversion strategy used in this paper works optimally for the considered tests, it is not necessarily the best general approach for an arbitrary set of observations. Based on the experience acquired with these tests, it seems advisable to approach the inversion of real spectropolarimetric data using different inversion strategies in order to find the optimal one.

While the inversion of thermodynamic quantities inferred from just the intensity profile is not new (e.g., Socas-Navarro et al. 2015; de la Cruz Rodríguez et al. 2019; Sainz Dalda et al. 2019), it is an important check that every inversion code must pass before advancing to the next step of inferring the magnetic field vector by full Stokes inversion. In all our tests the inference of the thermodynamic quantities is achieved satisfactorily in the range of heights corresponding to the region of formation of the Mg II h and k lines, including the extended wings whose presence is due to the PRD effects. The differences between the inferred and original models in this region of formation are likely due to model degeneracies among the parameters and to the different sensitivity of the emergent Stokes profiles

to them. Finally, it is important to observe that assuming hydrostatic equilibrium we are not directly inverting the stratification of the electron density, and the hydrogen populations are computed in LTE.

As we mentioned above, the inference of the magnetic field vector is significantly more complicated. In the Hanle regime (Zeeman splitting comparable to the natural width of the line), the longitudinal magnetic field component affects both the linear and circular spectral line polarization. As to the linear polarization, the extended wings of the Mg II h and k lines are sensitive to the longitudinal component of the magnetic field in the upper photosphere and low chromosphere (from $\log_{10}(\tau_{500}) \approx -3$ to $\log_{10}(\tau_{500}) \approx -4.5$); the circular polarization instead is sensitive to fields in the mid-upper chromosphere (from $\log_{10}(\tau_{500}) \approx -4.5$ to $\log_{10}(\tau_{500}) \approx -6$). Consequently, the longitudinal component of the magnetic field is satisfactorily inferred in the region of formation of the h and k lines of the model atmosphere.

The inference of the strength and azimuth of the transverse component of the magnetic field is less accurate. When the contribution of the Zeeman effect to the linear polarization in the core of the lines is negligible (as in our tests) only the linear polarization in the core of the Mg II k line is sensitive to the magnetic field vector via the Hanle effect. Because the line core forms in the upper chromosphere ($\log_{10}(\tau_{500}) \approx -7$ in the model) the inference of the stratification of the transverse field component is worse than for the longitudinal component. Nevertheless, the inferred values in the region of formation of the Mg II k line core are not far from the original ones. We note that the linear polarization in the troughs of the k line is also sensitive to the transverse component of the magnetic field via the Hanle effect, but its sensitivity to the longitudinal magnetic field component via the magneto-optical effects is much more significant. The magnetic field azimuth is the parameter that has shown the strongest dependence on the inversion strategy and, while the inferred values are often close to the original ones, we also get errors up to 40° (see Fig. 3) in some cases, making this the less reliable of the inferred parameters.

We have also tested the performance of the TIC by adding photon noise to the input data. As expected, the uncertainty associated with the inversion (see Eq. (2)) increases and the transverse field and its azimuth are the most affected parameters. Even though the inverted stratification of the transverse field is strongly impacted by the presence of polarimetric noise (see Fig. 6), around the formation height where the line is sensitive to the field (between $\log_{10}(\tau_{500}) \approx -5.0$ and ≈ -6.5) the inferred magnetic strength with and without noise are reasonably close.

Finally, we presented an application where only the circular polarization is used to infer the longitudinal component of the magnetic field. An important conclusion is that the atomic alignment produced by the anisotropy of the radiation field has a significant impact on the inferred field strength, which can lead to overestimating the actual strength of the magnetic field. Given that this impact of the radiation field anisotropy to the circular polarization is consequence of the PRD effects (del Pino Alemán et al. 2016; Alsina Ballester et al. 2016), we emphasize that accounting for photon coherence effects is also crucial for the a reliable inference of the magnetic field stratification.

In conclusion, the tests and results shown in this paper demonstrate that our TIC code provides a viable inversion strategy to attack the complex problem of the generation and transfer of polarization in strong resonance lines of the chromosphere and transition region. This paves the way toward the application of TIC to the inversion of the exciting new spectropolarimetric observations provided by the CLASP2 missions, as well as future mission concepts currently under development, such as the Chromospheric Magnetism Explorer (CMEx) and the Solar Transition UV Explorer (STRUVE). The inversion of CLASP2 data with TIC is under way, with very promising preliminary results that will be the subject of future publications. In parallel, we will keep improving TIC and make it available to the community once the public version of the HanleRT forward engine is released.

ACKNOWLEDGMENTS

We thank Andrés Asensio Ramos and Basilio Ruiz Cobo for helpful discussions, and Rebecca Centeno and Han Uitenbroek for useful suggestions and comments. We acknowledge the funding received from the European Research Council (ERC) under the European Union’s Horizon 2020 research and innovation programme (ERC Advanced Grant agreement No 742265). This material is based upon work supported by the National Center for Atmospheric Research, which is a major facility sponsored by the National Science Foundation under Cooperative Agreement No. 1852977.

REFERENCES

- | | |
|--|--|
| <p>Alsina Ballester, E., Belluzzi, L., & Trujillo Bueno, J. 2016, ApJL, 831, L15, doi: 10.3847/2041-8205/831/2/L15</p> | <p>Asensio Ramos, A., Trujillo Bueno, J., & Landi Degl’Innocenti, E. 2008, ApJ, 683, 542, doi: 10.1086/589433</p> |
|--|--|

- Belluzzi, L., & Trujillo Bueno, J. 2012, *ApJL*, 750, L11, doi: [10.1088/2041-8205/750/1/L11](https://doi.org/10.1088/2041-8205/750/1/L11)
- . 2014, *A&A*, 564, A16, doi: [10.1051/0004-6361/201321598](https://doi.org/10.1051/0004-6361/201321598)
- Belluzzi, L., Trujillo Bueno, J., & Štěpán, J. 2012, *ApJL*, 755, L2, doi: [10.1088/2041-8205/755/1/L2](https://doi.org/10.1088/2041-8205/755/1/L2)
- Carlsson, M., De Pontieu, B., & Hansteen, V. H. 2019, *ARA&A*, 57, 189, doi: [10.1146/annurev-astro-081817-052044](https://doi.org/10.1146/annurev-astro-081817-052044)
- Casini, R., del Pino Alemán, T., & Manso Sainz, R. 2017a, *ApJ*, 835, 114, doi: [10.3847/1538-4357/835/2/114](https://doi.org/10.3847/1538-4357/835/2/114)
- . 2017b, *ApJ*, 848, 99, doi: [10.3847/1538-4357/aa8a73](https://doi.org/10.3847/1538-4357/aa8a73)
- Casini, R., Landi Degl’Innocenti, M., Manso Sainz, R., Landi Degl’Innocenti, E., & Landolfi, M. 2014, *ApJ*, 791, 94, doi: [10.1088/0004-637X/791/2/94](https://doi.org/10.1088/0004-637X/791/2/94)
- de la Cruz Rodríguez, J., Leenaarts, J., & Asensio Ramos, A. 2016, *ApJL*, 830, L30, doi: [10.3847/2041-8205/830/2/L30](https://doi.org/10.3847/2041-8205/830/2/L30)
- de la Cruz Rodríguez, J., Leenaarts, J., Danilovic, S., & Uitenbroek, H. 2019, *A&A*, 623, A74, doi: [10.1051/0004-6361/201834464](https://doi.org/10.1051/0004-6361/201834464)
- de la Cruz Rodríguez, J., & van Noort, M. 2017, *SSRv*, 210, 109, doi: [10.1007/s11214-016-0294-8](https://doi.org/10.1007/s11214-016-0294-8)
- De Pontieu, B., Title, A. M., Lemen, J. R., et al. 2014, *SoPh*, 289, 2733, doi: [10.1007/s11207-014-0485-y](https://doi.org/10.1007/s11207-014-0485-y)
- del Pino Alemán, T., Casini, R., & Manso Sainz, R. 2016, *ApJL*, 830, L24, doi: [10.3847/2041-8205/830/2/L24](https://doi.org/10.3847/2041-8205/830/2/L24)
- del Pino Alemán, T., Trujillo Bueno, J., Casini, R., & Manso Sainz, R. 2020, *ApJ*, 891, 91, doi: [10.3847/1538-4357/ab6bc9](https://doi.org/10.3847/1538-4357/ab6bc9)
- del Pino Alemán, T., Trujillo Bueno, J., Štěpán, J., & Shchukina, N. 2018, *ApJ*, 863, 164, doi: [10.3847/1538-4357/aaceab](https://doi.org/10.3847/1538-4357/aaceab)
- del Toro Iniesta, J. C. 2003, *Introduction to Spectropolarimetry*
- del Toro Iniesta, J. C., & Ruiz Cobo, B. 2016, *Living Reviews in Solar Physics*, 13, 4, doi: [10.1007/s41116-016-0005-2](https://doi.org/10.1007/s41116-016-0005-2)
- Fontenla, J. M., Avrett, E. H., & Loeser, R. 1993, *ApJ*, 406, 319, doi: [10.1086/172443](https://doi.org/10.1086/172443)
- Ishikawa, R., Bueno, J. T., del Pino Alemán, T., et al. 2021, *Science Advances*, 7, eabe8406, doi: [10.1126/sciadv.abe8406](https://doi.org/10.1126/sciadv.abe8406)
- Jaume Bestard, J., Trujillo Bueno, J., Štěpán, J., & del Pino Alemán, T. 2021, *ApJ*, 909, 183, doi: [10.3847/1538-4357/abd94a](https://doi.org/10.3847/1538-4357/abd94a)
- Kano, R., Trujillo Bueno, J., Winebarger, A., et al. 2017, *ApJL*, 839, L10, doi: [10.3847/2041-8213/aa697f](https://doi.org/10.3847/2041-8213/aa697f)
- Lagg, A., Lites, B., Harvey, J., Gosain, S., & Centeno, R. 2017, *SSRv*, 210, 37, doi: [10.1007/s11214-015-0219-y](https://doi.org/10.1007/s11214-015-0219-y)
- Landi Degl’Innocenti, E., & Landolfi, M. 2004, *Polarization in Spectral Lines*, Vol. 307, doi: [10.1007/978-1-4020-2415-3](https://doi.org/10.1007/978-1-4020-2415-3)
- Magain, P. 1986, *A&A*, 163, 135
- Manso Sainz, R., del Pino Alemán, T., Casini, R., & McIntosh, S. 2019, *ApJL*, 883, L30, doi: [10.3847/2041-8213/ab412c](https://doi.org/10.3847/2041-8213/ab412c)
- Manso Sainz, R., & Trujillo Bueno, J. 2011, *ApJ*, 743, 12, doi: [10.1088/0004-637X/743/1/12](https://doi.org/10.1088/0004-637X/743/1/12)
- Mihalas, D. 1970, *Stellar atmospheres*
- Milić, I., & van Noort, M. 2017, *A&A*, 601, A100, doi: [10.1051/0004-6361/201629980](https://doi.org/10.1051/0004-6361/201629980)
- . 2018, *A&A*, 617, A24, doi: [10.1051/0004-6361/201833382](https://doi.org/10.1051/0004-6361/201833382)
- Press, W. H., Teukolsky, S. A., Vetterling, W. T., & Flannery, B. P. 2007, *Numerical Recipes 3rd Edition: The Art of Scientific Computing*, 3rd edn. (Cambridge University Press)
- Ruiz Cobo, B., & del Toro Iniesta, J. C. 1992, *ApJ*, 398, 375, doi: [10.1086/171862](https://doi.org/10.1086/171862)
- Ruiz Cobo, B., Quintero Noda, C., Gafeira, R., et al. 2022, *A&A*, 660, A37, doi: [10.1051/0004-6361/202140877](https://doi.org/10.1051/0004-6361/202140877)
- Sainz Dalda, A., de la Cruz Rodríguez, J., De Pontieu, B., & Gošić, M. 2019, *ApJL*, 875, L18, doi: [10.3847/2041-8213/ab15d9](https://doi.org/10.3847/2041-8213/ab15d9)
- Sánchez Almeida, J. 1997, *ApJ*, 491, 993, doi: [10.1086/304999](https://doi.org/10.1086/304999)
- Socas-Navarro, H., de la Cruz Rodríguez, J., Asensio Ramos, A., Trujillo Bueno, J., & Ruiz Cobo, B. 2015, *A&A*, 577, A7, doi: [10.1051/0004-6361/201424860](https://doi.org/10.1051/0004-6361/201424860)
- Socas-Navarro, H., Trujillo Bueno, J., & Ruiz Cobo, B. 2000, *ApJ*, 530, 977, doi: [10.1086/308414](https://doi.org/10.1086/308414)
- Trujillo Bueno, J. 2001, in *Astronomical Society of the Pacific Conference Series*, Vol. 236, *Advanced Solar Polarimetry – Theory, Observation, and Instrumentation*, ed. M. Sigwarth, 161. <https://arxiv.org/abs/astro-ph/0202328>
- Trujillo Bueno, J., & del Pino Alemán, T. 2022, *ARA&A*, 60, in press
- Trujillo Bueno, J., Štěpán, J., & Casini, R. 2011, *ApJL*, 738, L11, doi: [10.1088/2041-8205/738/1/L11](https://doi.org/10.1088/2041-8205/738/1/L11)
- Trujillo Bueno, J., Štěpán, J., Belluzzi, L., et al. 2018, *ApJL*, 866, L15, doi: [10.3847/2041-8213/aae25a](https://doi.org/10.3847/2041-8213/aae25a)
- Uitenbroek, H. 2006, in *Astronomical Society of the Pacific Conference Series*, Vol. 354, *Solar MHD Theory and Observations: A High Spatial Resolution Perspective*, ed. J. Leibacher, R. F. Stein, & H. Uitenbroek, 313
- Štěpán, J., & Trujillo Bueno, J. 2016, *ApJL*, 826, L10, doi: [10.3847/2041-8205/826/1/L10](https://doi.org/10.3847/2041-8205/826/1/L10)

Štěpán, J., Trujillo Bueno, J., Leenaarts, J., & Carlsson, M.
2015, ApJ, 803, 65, doi: [10.1088/0004-637X/803/2/65](https://doi.org/10.1088/0004-637X/803/2/65)

Wittmann, A. 1974, SoPh, 35, 11, doi: [10.1007/BF00156952](https://doi.org/10.1007/BF00156952)